Neutrophils from p40$^{phox-/-}$ mice exhibit severe defects in NADPH oxidase regulation and oxidant-dependent bacterial killing

Chris D. Ellson,[1] Keith Davidson,[1] G. John Ferguson,[1] Rod O'Connor,[2] Len R. Stephens,[1] and Phillip T. Hawkins[1]

[1]Inositide Laboratory and [2]Laboratory of Molecular Signalling, The Babraham Institute, Babraham Research Campus, Cambridge CB2 4AT, UK

The generation of reactive oxygen species (ROS) by the reduced nicotinamide adenine dinucleotide phosphate (NADPH) oxidase complex plays a critical role in the antimicrobial functions of the phagocytic cells of the immune system. The catalytic core of this oxidase consists of a complex between gp91^{phox}, p22^{phox}, p47^{phox}, p67^{phox}, p40^{phox}, and rac-2. Mutations in each of the *phox* components, except p40^{phox}, have been described in cases of chronic granulomatous disease (CGD), defining their essential role in oxidase function. We sought to establish the role of p40^{phox} by investigating the NADPH oxidase responses of neutrophils isolated from p40$^{phox-/-}$ mice. In the absence of p40^{phox}, the expression of p67^{phox} is reduced by ~55% and oxidase responses to tumor necrosis factor α/fibrinogen, immunoglobulin G latex beads, *Staphylococcus aureus*, formyl-methionyl-leucyl-phenylalanine, and zymosan were reduced by ~97, 85, 84, 75, and 30%, respectively. The defect in ROS production by p40$^{phox-/-}$ neutrophils in response to *S. aureus* translated into a severe, CGD-like defect in the killing of this organism both in vitro and in vivo, defining p40^{phox} as an essential component in bacterial killing.

CORRESPONDENCE
Phillip T. Hawkins:
phillip.hawkins@bbsrc.ac.uk

Abbreviations used: BMN, bone marrow–derived neutrophil; CGD, chronic granulomatous disease; DPI, diphenyleneiodonium chloride; HRP, horseradish peroxidase; MAPK, mitogen-activated protein kinase; NADPH, reduced nicotinamide adenine dinucleotide phosphate; NBT, nitroblue tetrazolium; PI3K, phosphoinositide 3-kinase; ROS, reactive oxygen species.

The reduced nicotinamide adenine dinucleotide phosphate (NADPH) oxidase of neutrophils and macrophages plays an essential role in the mechanisms by which these cells destroy engulfed pathogens (1, 2). The delivery of superoxide anion (O_2^-) by this enzyme complex into the phagosome is thought to indirectly activate several classes of protease (3), and O_2^- itself can be directly converted into a variety of destructive molecular species (reactive oxygen species [ROS] and halide derivatives) (4, 5). Together with the delivery of other nonoxidant-dependent microbicidal agents into the phagosome, e.g., defensins (6), the NADPH oxidase plays a central role in our defense mechanisms against invading microbes.

Although the role of the phagocyte NADPH oxidase in microbe killing is clear, it has become apparent that the same, or closely homologous, enzyme complexes also exist in many other cell types, e.g., in lymphocytes and endothelia (1, 5, 7). The role of ROS produced by the NADPH oxidases in these other cell types is still largely undefined but is likely to include intra- and peri-cellular signaling via H_2O_2-mediated oxidation of critical cysteine residues in target proteins. Thus far, these target proteins are largely thought to be members of the protein tyrosine phosphate phosphatase superfamily that are intermediaries in cell surface receptor–regulated signaling pathways (8).

The core molecular components of the phagocyte NADPH oxidase are a b-type membrane-bound cytochrome consisting of gp91^{phox} and p22^{phox} subunits (cytochrome b_{558}) and four soluble components: rac-2, p67^{phox}, p47^{phox}, and p40^{phox} (1, 2). On activation, the soluble components form an active complex with the b-type cytochrome and electrons are transferred from NADPH, across the membrane, and are delivered to molecular oxygen to generate the superoxide anion, O_2^-. The importance of the NADPH oxidase is clearly witnessed by molecular defects in components of the NADPH oxidase, which lead to chronic granulomatous disease (CGD), a genetic disorder in which patients suffer recurrent fungal and bacterial

C.D. Ellson and K. Davidson contributed equally to this work.
The online version of this article contains supplemental material.

infections (9, 10). Additionally, a phagocyte immunodeficiency has also been described in a patient with dysfunctional rac-2 (11). The molecular events that underlie NADPH oxidase activation are still incompletely understood, but there is now overwhelming evidence that key aspects are GTP-rac-2 binding to $p67^{phox}$ and multiple phosphorylation of $p47^{phox}$ (1, 2, 12), which promote complex formation with each other and the cytochrome to form a catalytically competent enzyme.

There is a very large range of stimuli that activate the oxidase in cells such as neutrophils and macrophages, and hence there is a large variety of receptor subtypes and associated signaling pathways that underlie this capability. Microbes are phagocytosed via a series of overlapping and redundant receptors, such as members of the integrin and antibody receptor families, depending on the organisms themselves and the type and degree of opsonization (13, 14), resulting in subsequent activation of NADPH oxidase on both the plasma and phagosomal membranes. Cells such as neutrophils also undergo rapid activation of their NADPH oxidase in response to soluble stimuli, such as formylated peptides (e.g., FMLP), leukotrienes (e.g., LTB4), and components of complement (C5a) (15). Furthermore, a variety of other inflammatory agents, which include cytokines such as TNF-α, GM-CSF, IL-8, and low doses of the primary stimuli themselves, collectively "prime" the oxidase, resulting in substantial upregulation of NADPH oxidase activity in response to primary stimuli at the site of inflammation (15–17). As a consequence, a very large number of intracellular signaling pathways have been shown to influence NADPH oxidase activation. Progress has been made defining some of these pathways, e.g., the coupling of receptor activation to guanine nucleotide exchange on rac (18–21) and protein kinase C–mediated phosphorylation on $p47^{phox}$ (22–24 and previous references), but it is already clear that these sit within a web of yet more, ill-defined regulatory inputs into the oxidase. For example, it is known that several oxidase components are the targets of complex patterns of phosphorylation and phospholipid binding driven by mitogen-activated protein kinase (MAPK) and phosphoinositide 3-kinase (PI3K) signaling pathways (25–31).

Among the NADPH oxidase subunits, $p40^{phox}$ is perhaps the least well understood. It is known to bind $p67^{phox}$ via reciprocal PB1 domain dimerization (32, 33), forming a tight complex in the cytosol of resting neutrophils (34, 35); however, there is some debate as to whether it is also found in a trimeric complex with $p67^{phox}$ and $p47^{phox}$ or whether this complex only occurs on activation or priming (22, 36, 37). $p40^{phox}$ is not required to reconstitute anionic detergent-stimulated oxidase activity in recombinant assays (34), and mutations in the $p40^{phox}$ gene have not been described in cases of CGD, leading to the view that it is not essential for NADPH oxidase activity. There are several reports, however, that suggest that, under some assay conditions, $p40^{phox}$ can influence oxidase activity in vitro (37–40) and several conflicting reports using cell-based assays that have suggested that $p40^{phox}$ is either a positive or negative regulator of the NADPH oxidase (41–43). $p40^{phox}$ has a clearly defined domain structure (PX, PB1, and SH3 domains) that is evolutionarily conserved and undergoes stimulated phosphorylation paralleling NADPH oxidase activation (44, 45). The PX domain has high specificity and affinity for binding the class III PI3K product PtdIns3P (37, 46, 47), but the physiological relevance of this interaction has yet to be shown in vivo. Similarly, the SH3 domain has been shown to bind a polyproline motif in $p47^{phox}$ with low affinity, but the true in vivo ligand for this domain has yet to be conclusively identified (36, 48, 49). Furthermore, although several binding partners for $p40^{phox}$ have been described, including moesin (50), coronin (51), thioredoxin (52), and Ku70 (53), these have not immediately provided a molecular explanation for the role of $p40^{phox}$. To define the requirement for $p40^{phox}$ in NADPH oxidase regulation, we have created mice with a lesion in the $p40^{phox}$ gene and present the first characterization of NADPH oxidase activation and bacterial killing in neutrophils from $p40^{phox-/-}$ animals.

RESULTS

$p40^{phox-/-}$ mice are viable and produce differentiated neutrophils

$p40^{phox-/-}$ mice were produced by standard gene-targeting strategies (see Materials and methods and Fig. S1 A, which is available at http://www.jem.org/cgi/content/full/jem.20052069/DC1). Two independent embryonic stem cell lines were used to derive two independent strains of $p40^{phox-/-}$ mice. These two strains could not be distinguished on the basis of any of the experiments presented, and, where appropriate, data is compiled from several animals of each strain. $p40^{phox-/-}$, $p40^{phox+/-}$, and $p40^{phox+/+}$ animals were produced from the breeding of $p40^{phox+/-}$ heterozygotes in the expected Mendelian ratios and appeared healthy and fertile when kept under barrier conditions. $p40^{phox-/-}$ mice had normal organ weights (Fig. S2, available at http://www.jem.org/cgi/content/full/jem.20052069/DC1) and normal blood cell counts (Fig. 1 A).

We used a mouse monoclonal antibody to $p40^{phox}$ to investigate the tissue distribution of $p40^{phox}$ protein. Amongst the tissues examined, we could only find strong evidence for immuno-detectable protein that was absent in equivalent $p40^{phox-/-}$ samples (Fig. 1 B, arrowheads) in both bone marrow–derived neutrophils (BMNs) and in the spleen, suggesting that $p40^{phox}$ expression is highly restricted. We could not detect expression of $p40^{phox}$ in BMNs from $p40^{phox-/-}$ mice using three different monoclonal and polyclonal antibodies raised against $p40^{phox}$ (Fig. 1 C and unpublished data), indicating successful targeting of the $p40^{phox}$ gene. Expression of $p47^{phox}$ was unaffected by the absence of $p40^{phox}$, but expression of $p67^{phox}$ was significantly reduced (Fig. 1 C). Careful quantitation indicated that $p67^{phox}$ levels in BMNs from $p40^{phox-/-}$ mice were reduced to 44.8 ± 4.3% of wild-type levels (Fig. 1 E). $p40^{phox+/-}$ BMNs demonstrated 71.9 ± 3.9% and 15.3 ± 4.0% reductions in $p40^{phox}$ and $p67^{phox}$, respectively (Fig. 1, D and E).

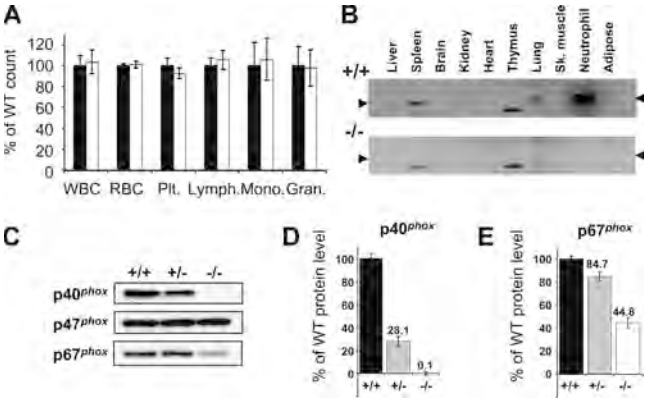

Figure 1. Blood cell counts and *phox* protein expression in p40$^{phox-/-}$ mice. (A) Peripheral blood from p40$^{phox+/+}$ and p40$^{phox-/-}$ animals was analyzed in a Vetabc animal blood cell counter. WBC, white blood cells; RBC, red blood cells; Plt, platelets, Lymph, lymphocytes; Mono, monocytes; Gran, granulocytes. Data represented are mean percentage of wild-type counts ± SE (n = 12). (B) 30 μg of clarified, homogenized tissues from p40$^{phox+/+}$ and p40$^{phox-/-}$ animals was subjected to SDS-PAGE and immunoblotted for p40^{phox}. Arrowheads indicate position of p40^{phox}. We routinely observed immunoreactive bands in the spleen and thymus from p40$^{phox-/-}$ animals. We do not know whether they are products of alternative splicing of p40^{phox} gene transcripts. (C) BMNs from p40$^{phox+/+}$, p40$^{phox+/-}$, and p40$^{phox-/-}$ animals were sonicated into SDS sample buffer, subjected to SDS-PAGE, and immunoblotted for p40^{phox}, p47^{phox}, and p67^{phox}. Graphs represent quantitation of p40^{phox} (D) and p67^{phox} (E) levels in BMNs as mean percentage of wild-type samples ± SE (n = 10–13) from 6–10 independent experiments using three to six mice per preparation.

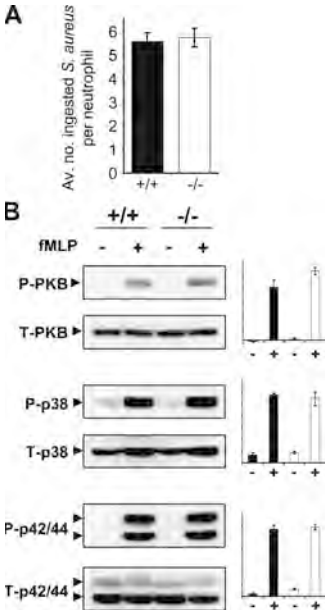

Figure 2. p40$^{phox-/-}$ neutrophils exhibit normal *S. aureus* phagocytosis and FMLP-induced signal transduction. (A) Primed p40$^{phox+/+}$ and p40$^{phox-/-}$ BMNs were adhered to glass and allowed to phagocytose serum-opsonized, FITC-labeled *S. aureus* for 40 min. Coverslips were washed and fixed, and the mean number of internalized bacteria per neutrophil was determined. 300 neutrophils were examined (n = 2). (B) p40$^{phox+/+}$ and p40$^{phox-/-}$ BMNs were incubated for 1min in the presence (+) or absence (−) of 10 μM FMLP. Resultant lysates were split between two blots and probed with phospho- (P) and total (T) antibodies against PKB, p38 MAPK, and p42/44 Erk. Graphs represent quantification of phospho-protein levels ± the range from a single experiment representative of three experiments. Black bars, +/+; white bars, −/−. Units are arbitrary.

BMNs from p40$^{phox-/-}$ mice were able to support normal phagocytic uptake of *Staphylococcus aureus* (Fig. 2 A) and zymosan (unpublished data), and normal activation of PKB, p38 MAPK, and p42/44 MAPK in response to FMLP (Fig. 2 B). These results suggest that the functions of several receptor classes characteristic of differentiated neutrophils are intact in BMNs from p40$^{phox-/-}$ mice.

p40$^{phox-/-}$ neutrophils show substantially reduced oxidase activation in response to several soluble stimuli

We characterized production of ROS in response to FMLP in either unprimed, mTNF-α–, or mGM-CSF–primed BMNs isolated from p40$^{phox-/-}$, p40$^{phox+/-}$, and p40$^{phox+/+}$ mice. ROS production was measured by a horseradish peroxidase (HRP)-dependent chemiluminescence assay that provides a rate measure of O_2^- production into the extracellular space. ROS production under each of these circumstances was severely reduced in the p40$^{phox-/-}$ mice (~69–84% defective; Fig. 3, A–C). The kinetics of the remaining ROS production were similar in p40$^{phox-/-}$ neutrophils compared with the wild-type, and the dose-response curves to FMLP showed only a small shift to higher concentrations (Fig. 3, A–C). PMA is often used to bypass cell surface receptors and induce a more direct activation of the NADPH oxidase via, amongst less well-defined pathways, a direct protein kinase C–mediated phosphorylation of p47^{phox}. PMA-induced production of ROS in p40$^{phox-/-}$ neutrophils was also substantially reduced compared with the wild-type (Fig. 3 D) and showed negligible shifts in the dose-response curves.

p40$^{phox-/-}$ neutrophils show variable reductions in oxidase activation in response to different particulate stimuli

We characterized ROS responses in both primed and unprimed BMNs from p40$^{phox-/-}$ and p40$^{pho+/+}$ mice in response to various particulate stimuli. We initially measured ROS production using luminol-dependent luminescence in the absence of HRP, which previous work has indicated is a rate measure of ROS production in the vicinity of endogenous peroxidases, largely thought to arise from the coincident deposition of ROS and myeloperoxidase into the phagosome (54). This is supported by our own data indicating little effect of adding extracellular HRP in these assays (unpublished data). Under these circumstances, there were significant differences in the relative reductions in ROS production seen with p40$^{phox-/-}$ neutrophils compared with the wild-type, depending on the nature of the stimulus (Fig. 4).

Priming the cells with mTNF-α and mGM-CSF caused a significant but relatively minor increase in the rate of ROS

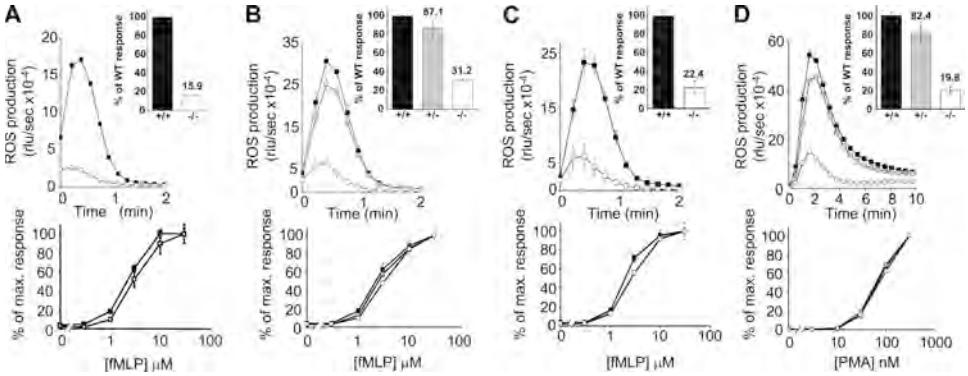

Figure 3. p40$^{phox-/-}$ neutrophils have severe defects in ROS production in response to soluble stimuli. BMNs from p40$^{phox+/+}$, p40$^{phox+/-}$, and p40$^{phox-/-}$ animals were analyzed for soluble stimulus-induced ROS production using HRP-dependent, luminol-dependent chemiluminescence. Duplicate wells of BMNs (3.75×10^5/well) were stimulated in a luminometer and ROS production (measured in relative light units per second, rlu/sec) was followed over time. 10 μM of unprimed FMLP (A), 10 μM mTNF-α–primed FMLP (B), 10 μM mGM-CSF–primed FMLP (C), and 300 nM PMA (D). Response kinetics (top line graph), total integrated responses as percentage of wild-type (bar graph), and agonist dose-response curves (bottom graph) are shown. Dose-response curves are standardized to 100% with 300 nM PMA and 30 μM FMLP, respectively. Black, +/+; gray, +/−; white, −/−. All data are means ± SE ($n = 6$) from three independent experiments using three to six mice per preparation.

generation in response to both unopsonized and opsonized zymosan and *S. aureus*, and a major increase in both the rate and magnitude of ROS generation in response to IgG latex beads. Looking across the full range of the responses to the various stimuli, the deficiencies in ROS production in the p40$^{phox-/-}$ versus p40$^{phox+/+}$ neutrophils were similar between the primed and unprimed cells (Fig. 4 A and unpublished data), suggesting that the p40^{phox} deficiency was not correlated with a specific deficiency in this type of priming mechanism.

Opsonization of zymosan with IgG or serum increased slightly the rate of ROS generation relative to the unopsonized particles but made relatively little difference to the level of the defect in the p40$^{phox-/-}$ versus p40$^{phox+/+}$ neutrophils (Fig. 4 and not depicted). Serum opsonization of *S. aureus* increased significantly the rate and magnitude of ROS production in response to these stimuli but again made relatively little difference to the level of defect in the p40$^{phox-/-}$ neutrophils (Fig. 4). The ROS responses to *S. aureus*, however, were much more affected by the loss of p40^{phox} than the responses to zymosan. The amounts of ROS produced by these stimuli over 2 h, across several experiments, are presented in Fig. 4 B (~84 vs. 30% defective for *S. aureus* and zymosan, respectively). These differences remained when varying amounts of these two stimuli were used (unpublished data), indicating a fundamental difference in their relative sensitivity to the loss of p40^{phox}. Zymosan and *S. aureus*, even in their unopsonized states, represent complex stimuli with respect to the receptors they engage; thus, this difference cannot at this stage be ascribed to particular receptor-associated signaling mechanisms. In an attempt to provide a phagocytic stimulus with a defined mechanism of entry, we made use of latex beads coated with IgG. Under the conditions of our assays, the ROS response to these beads was highly dependent on the IgG coating (Fig. 4); thus, it is reasonable to assume that an Fc receptor of some type plays a central role in the ROS response to this stimulus. p40$^{phox-/-}$ neutrophils exhibited a very severe defect in ROS production to IgG latex beads (~85%; Fig. 4), indicating that the signaling pathways from Fc receptors to the oxidase are highly dependent on p40^{phox}.

Given the requirement for both ROS and peroxidase activity in the luminol-dependent chemiluminescence assay, and the potential ambiguity in interpretation of a deficiency that this measurement provides, we also sought to measure NADPH oxidase activity in p40$^{phox-/-}$ and p40$^{phox+/+}$ neutrophils by measuring the rate of O_2 consumption. It has been shown previously that NADPH oxidase–catalyzed consumption of O_2 during a stimulated "respiratory burst" dominates O_2 consumption by other routes, e.g., mitochondrial respiration (55), and hence provides a measure of substrate use that should be independent of the location of the oxidase or the pathways of ROS use. PMA-, IgG-Zym–, and *S. aureus*–stimulated O_2 consumption showed similar relative differences between p40$^{phox+/+}$ and p40$^{phox-/-}$ BMNs as those previously described by the chemiluminescence measurements (Fig. 5, A and B). Thus, the p40$^{phox-/-}$ neutrophils showed large deficiencies in O_2 consumption when challenged with PMA and *S. aureus* yet a relatively minor deficiency when challenged with zymosan, despite similar absolute rates of O_2 consumption for each stimulus (Fig. 5 A).

To confirm that ROS accumulation by p40$^{phox-/-}$ BMNs in response to IgG-Zym was directed into the phagosome, we took advantage of the fact that O_2^--catalyzed reduction of soluble formazan salts to form insoluble, colored products can be used as a semiquantitative assay for the location of NADPH oxidase activity. Substantial formation of dark purple nitroblue tetrazolium (NBT) deposits could be seen in

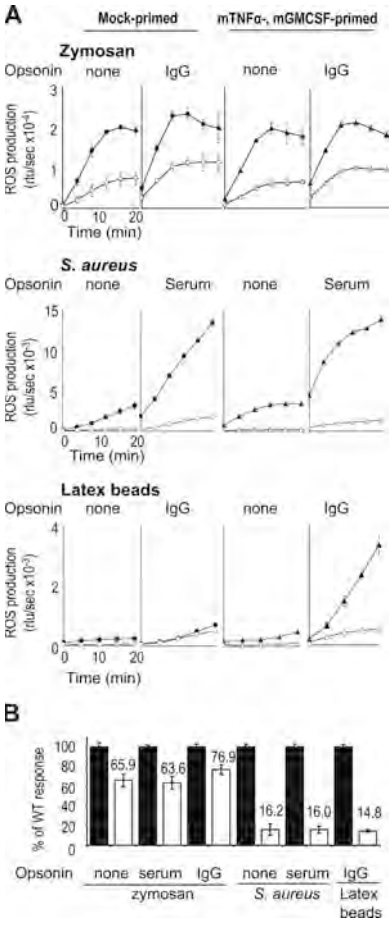

Figure 4. p40$^{phox-/-}$ neutrophils have differing defects in ROS production in response to particulate stimuli. BMNs from p40$^{phox+/+}$ and p40$^{phox-/-}$ animals were analyzed for particulate stimulus-induced ROS production using luminol-dependent chemiluminescence (filled symbols, +/+; open symbols, −/−). Triplicate wells of mock-primed or mTNF-α–, mGM-CSF–primed BMNs (3.75 × 10^5 BMN/well for *S. aureus* and zymosan stimulations, 1.25 × 10^6/well for latex beads stimulations) were stimulated in a luminometer and ROS production (measured in relative light units per second, rlu/sec) was followed over time (A). Each horizontal panel of graphs is shown on the same scale. Data are means ± SD from a single experiment representative of two to five independent experiments. Particles were either unopsonized or opsonized with IgG or mouse serum. Particle/BMN ratios are as follows: zymosan, 5:1; *S. aureus*, 20:1; IgG latex beads, 50:1. (B) Total integrated responses of primed BMNs to different stimuli over 2 h are shown as a percentage of wild-type. Black, +/+; white, −/−. Data are means ± SE (n = 6–10) from two to five independent experiments using three to six mice per preparation.

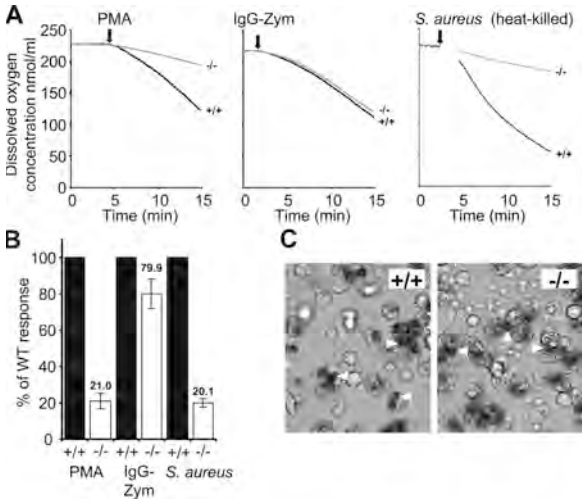

Figure 5. NADPH oxidase responses of p40$^{phox-/-}$ neutrophils assessed by measuring oxygen consumption and phagosomal NBT deposition. Oxygen consumption of BMNs from p40$^{phox+/+}$ and p40$^{phox-/-}$ animals, in response to various stimuli, was measured in a Clark-type oxygen electrode. Primed BMNs (5 × 10^6/ml) were prewarmed in the oxygen electrode chamber, stimuli were added, and oxygen consumption was followed over time. Line graphs (A) are typical examples of each stimulus: 1 μM PMA, IgG-Zym (20 particles per neutrophil), and heat-killed *S. aureus* (20 bacteria per neutrophil). *S. aureus* was heat killed before addition, as oxygen consumption by live bacteria dominated the neutrophil respiratory burst (unpublished data). BMNs were primed before IgG-Zym and *S. aureus* stimulation. (B) Quantification of rates of oxygen consumption as a percentage of wild-type, after deduction of prestimulus rate of oxygen consumption. Data are means ± SE (n = 3–5) from three to five independent experiments using three to six mice per preparation. (C) Primed BMNs were adhered to glass in the presence of NBT, IgG-Zym was added, and superoxide production (evident by the deposition of dark purple formazan precipitate) was imaged microscopically. Arrowheads indicate examples of NBT$^+$ phagosomes. Images show typical results ~30 min after IgG-Zym addition (n = 5 experiments using three to six mice per preparation).

zymosan-containing phagosomes in both p40$^{phox+/+}$ and p40$^{phox-/-}$ neutrophils (Fig. 5 C), suggesting that substantial oxidase activity must be present in these structures.

p40$^{phox-/-}$ neutrophils adherent on fibrinogen cannot generate ROS in response to TNF-α

Neutrophils attached to a variety of surfaces via their cell surface integrins can generate substantial quantities of extracellular ROS in response to costimulation by cytokines (e.g., TNF-α), chemoattractants (e.g., FMLP), or Fc receptors (FcγRIII in murine neutrophils) (56–58). We investigated the ability of BMNs from p40$^{phox-/-}$ mice attached to a fibrinogen surface to produce ROS in response to mTNF-α, a response previously established to be dependent on β2 integrin engagement (59, 60). p40$^{phox-/-}$ neutrophils exhibited a remarkable deficiency in this response compared with their wild-type controls (96.7 ± 0.7% reduced; Fig. 6, A and C). Similar defects were seen upon costimulation with FMLP and mGM-CSF (unpublished data). p40$^{phox-/-}$ neutrophils also exhibited a severe deficiency in activation of their oxidase in response to direct cross-linking of their β2 integrins by an anti-β2 antibody (95.1 ± 2.7% reduced; Fig. 6, B and C), a response that recent work has suggested is probably mediated via cooperation between β2 integrin and FcγRIII activation (58). p40$^{phox-/-}$ neutrophils expressed normal levels of cell surface β2 integrins and demonstrated no defect in TNF-α–induced adhesion and spreading on fibrinogen (Fig. 6, D and E).

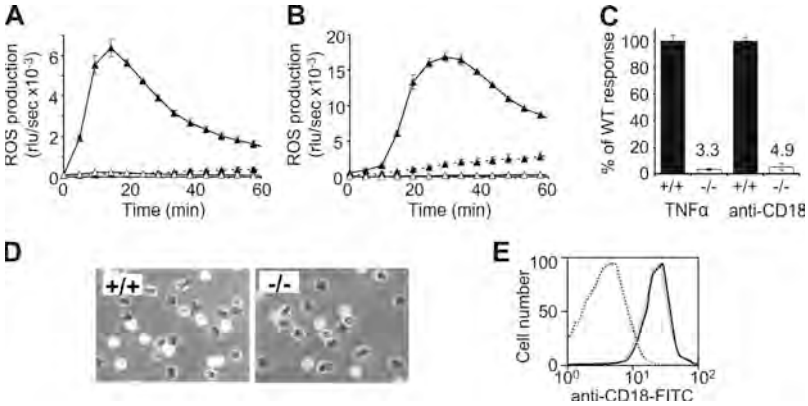

Figure 6. p40$^{phox-/-}$ neutrophils have severe deficiencies in adhesion-dependent ROS production. BMNs from p40$^{phox+/+}$ and p40$^{phox-/-}$ animals were analyzed for adhesion-dependent ROS production using HRP-dependent, luminol-dependent chemiluminescence on fibrinogen-coated plates (filled symbols, +/+; open symbols, −/−). Duplicate wells of BMNs (2.5×10^5/well) were stimulated in a luminometer and ROS production (measured in relative light units per second, rlu/sec) was followed over time. 20 ng/ml mTNF-α (A) and 18 μg/ml anti-CD18 (anti-β2 integrin) (B). Dotted lines are wild-type controls stimulated with buffer alone in A and IgG2a isotype control in B. Data are means ± range from a single experiment representative of three independent experiments. (C) Total integrated responses over 1 h as a percentage of wild-type. Data are means ± SE ($n = 6$) from three independent experiments. (D) Spreading responses on fibrinogen surfaces of TNF-α–stimulated neutrophils. Phase dark cells are considered spread. (E) Cell surface expression of CD18 in TNF-α–stimulated neutrophils. Solid lines are anti-CD18, and dotted lines are isotype controls. Black, +/+; gray, −/−. Data are from a single experiment representative of two independent experiments.

Thus, p40^{phox} plays an essential role in the pathways between integrin engagement and oxidase activation in these contexts of neutrophil activation.

p40$^{phox-/-}$ neutrophils exhibit a severe deficiency in bacterial killing in vitro

Killing of *S. aureus* by neutrophils in vitro is highly dependent on NADPH oxidase activity, consistent with the high frequency with which *S. aureus* infections present in cases of CGD (9, 10). In contrast, killing of *Escherichia coli* is relatively independent of neutrophil NADPH oxidase activity (61). In line with these conclusions, we found that the NADPH oxidase inhibitor diphenyleneiodonium chloride (DPI) had a much greater effect on the killing of *S. aureus* by BMNs than the killing of *E. coli* (Fig. 7, A and B). BMNs from p40$^{phox-/-}$ mice had a clear defect in the killing of *S. aureus* (~75% relative to wild-type) but an insignificant defect in the killing of *E. coli* (Fig. 7, A and B). This defect was mirrored in the killing of *S. aureus* by whole blood (Fig. S3, available at http://www.jem.org/cgi/content/full/jem.20052069/DC1). Using a range of DPI concentrations to construct a relationship between BMN NADPH oxidase activity and *S. aureus* killing (61), the NADPH oxidase deficiency of p40$^{phox-/-}$ neutrophils correlates well with their deficiency in *S. aureus* killing (Fig. 7 C), suggesting that the two are causally linked.

p40$^{phox-/-}$ mice are deficient in clearing an *S. aureus* infection in vivo

We sought to establish whether the substantial defect in the in vitro killing of *S. aureus* by p40$^{phox-/-}$ neutrophils translated into a defect in the killing of this organism in the whole animal. We injected live *S. aureus* into the peritoneum of p40$^{phox-/-}$ and p40$^{phox+/+}$ mice and measured the number of surviving bacteria over the subsequent 24 h. We reproducibly recovered significantly more live *S. aureus* from the p40$^{phox-/-}$ mice than their wild-type controls (Fig. 7 D).

DISCUSSION

We observed very substantial defects in NADPH oxidase activity in neutrophils isolated from p40$^{phox-/-}$ mice, defining an essential role for p40^{phox} in the physiological regulation of this important enzyme complex. The degree of defect in NADPH oxidase activity varied greatly depending on the nature of the stimulus. Large defects were observed in intracellular ROS production in response to *S. aureus* or IgG latex beads, and smaller defects were observed in response to the uptake of zymosan. Extracellular ROS generation was absent in response to TNF-α/fibrinogen and greatly reduced in response to FMLP or PMA. ROS stimulation by TNF-α/fibrinogen is thought to occur via costimulation of β2 integrins and TNF-α receptors (59, 62). FMLP is thought to activate the oxidase via formyl-peptide receptors (63) and IgG to act via Fcγ receptors (64). *S. aureus* and zymosan are complex stimuli that are engulfed and activate the oxidase through a combination of inaccurately defined receptor types, but these are likely to include β2 integrin receptors (64) and β glucan receptors (65). Furthermore, these receptor types are likely to be extended in vivo through opsonization with complement or antibodies. Thus, it is clear that loss of p40^{phox} has a differential impact in the signaling pathways from different receptor subtypes. The extent of p40^{phox} involvement in the various physiological mechanisms of NADPH oxidase activation in neutrophils and other cell types will only be resolved with much further work, but our in vitro and in vivo

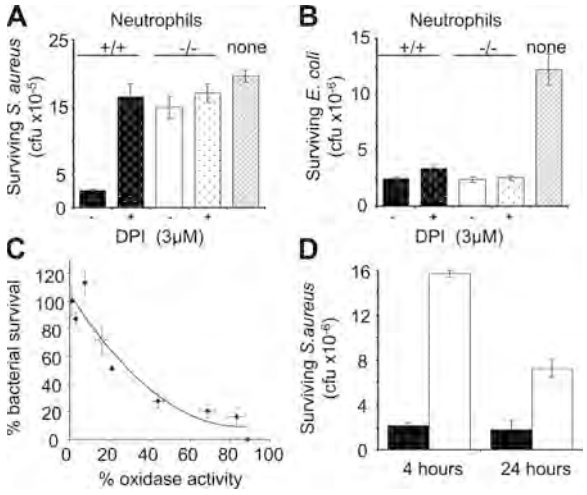

Figure 7. p40$^{phox-/-}$ neutrophils are severely deficient in killing of *S. aureus* in vitro and in vivo. (A and B) Primed BMNs from p40$^{phox+/+}$ and p40$^{phox-/-}$ animals were incubated for 15 min with serum-opsonized *S. aureus* (approximate ratio of 1 bacterium to 4 neutrophils) (A) or 5 min with serum-opsonized *E. coli* (approximate ratio of 1 bacterium to 1 neutrophil) (B) with rapid mixing. Samples were added to ice-cold LB-saponin and sonicated to liberate ingested bacteria. Surviving bacteria were enumerated by plating and subsequent counting of colonies. "No neutrophil" controls and controls with 3 μM DPI were also run. Data are means ± SD ($n = 3$) and representative of two to five experiments using three to six mice per preparation. (C) A dose curve of DPI (0.003–10 μM) was applied to wild-type mouse neutrophils in parallel luminometer-based ROS production assays in response to *S. aureus* and *S. aureus* killing assays. Resultant NADPH oxidase activity and *S. aureus* survival values were plotted against each other (filled symbols) and a trendline was fitted, representing the dependence of killing on NADPH oxidase activity in wild-type neutrophils. The data point for p40$^{phox-/-}$ neutrophils in response to *S. aureus* (bacterial killing vs. NADPH oxidase activity) was plotted on the same graph (open symbol). Data are means ± SE ($n = 6$) from two to three independent experiments using three to six mice per preparation. (D) Mice were injected intraperitoneally with 5×10^7 live *S. aureus*. After 4 or 24 h, mice were killed and peritoneums were flushed with ice-cold buffer. Aliquots were added to ice-cold LB-saponin, sonicated to liberate ingested bacteria, diluted, and plated, and surviving bacteria were enumerated. Total numbers of surviving bacteria per animal were calculated for each time point. Black, p40$^{phox+/+}$; white, p40$^{phox-/-}$. Data are means ± SE ($n = 3$ mice per time point) from a single experiment representative of three independent experiments.

models of oxidant-dependent bacterial killing already indicate that it is a critical component of our innate defense mechanism (Fig. 7). Importantly, the extent of the *S. aureus* killing defect is as severe as that observed with neutrophils from p47$^{phox-/-}$ CGD model mice (3, 66).

A key question is clearly the molecular mechanism by which p40^{phox} acts in the signaling pathways to NADPH oxidase activation. We observed that p67^{phox} levels are reduced by ~55% in p40$^{phox-/-}$ neutrophils. p67^{phox} and p40^{phox} are established to exist in a complex in neutrophils, although the stoichiometry and relative inclusion of p47^{phox} in the resting state are still in debate. In p67^{phox}-deficient CGD patients, p40^{phox} expression is reduced (34, 67, 68), suggesting that p40^{phox} and p67^{phox} mutually regulate each other's steady-state expression, and this is supported by the reduced p67^{phox} levels in p40$^{phox-/-}$ neutrophils. Whether this regulation occurs at the level of protein stability, mRNA stability, or transcriptional/translational control is unknown. It is established that p67^{phox} is an absolute requirement for reconstituted NADPH oxidase activity in vitro and, through characterized cases of CGD, also in vivo. Thus, the drop in p67^{phox} levels in the p40$^{phox-/-}$ neutrophils is a confounding issue in trying to ascribe molecular consequences to the loss of p40^{phox}. There is the possibility that this reduction in p67^{phox} has an impact directly on the oxidase, and there is also the possibility that this has an impact indirectly, via altering the dependence on other subunits. Unfortunately, the absence of a p67$^{phox-/-}$ mouse model prevents a simple assessment of this impact in p67$^{phox+/-}$ mice; however, we note that human carriers of p67^{phox}-deficient CGD do not present with a CGD phenotype (69). Further, the very large reductions in oxidase responses to TNF-α/fibrinogen and *S. aureus* in p40$^{phox-/-}$ neutrophils suggest that p40^{phox} has a substantial role in these responses under normal circumstances.

Earlier work has suggested that PtdIns3P binding to the PX domain of p40^{phox} may play a role linking PI3K signaling pathways to NADPH oxidase activation (22, 37, 46, 47). Furthermore, the discovery that PtdIns3P synthesis can occur on phagosomal membranes provided a context for this potential mechanism (70, 71). Evidence that this pathway does indeed operate in FcγRII receptor stimulation of the NADPH oxidase in the COS *phox* system is provided in an accompanying article by Suh et al. (on p. 1915 of this issue; reference 72). In this elegantly engineered cell model, an intact PtdIns3P-binding PX domain of p40^{phox} is shown to be required for FcγRII receptor–initiated phagosomal ROS production. Our data describing the very large reduction in IgG latex bead–stimulated ROS production in p40$^{phox-/-}$ neutrophils provides strong in vivo corroboration of this model. However, further work must clearly be done measuring elements of the known pathways to NADPH oxidase activation (e.g., p47^{phox}/p67^{phox}/p40^{phox} phosphorylation, p47^{phox}/p67^{phox}/rac-2 translocation to cytochrome b_{558}) before the molecular consequences of the absence of p40^{phox} can be properly ascribed, and it is likely that these will need to be done in the context of replenishment of p67^{phox} and/or knock-in mutations of p40^{phox} before clear answers emerge. However, the development of the p40$^{phox-/-}$ mouse does appear to offer a potential route to answering these questions.

The absence of examples of CGD patients characterized by mutations in p40^{phox} together with enigmatic data arising from attempts to reconstitute the NADPH oxidase in cellular and a-cellular systems lead to the general view that p40^{phox} does not have a critical role in NADPH oxidase activation. A counter argument arising from data describing widespread tissue expression of p40^{phox} suggested that this protein may have a wider role outside of phagocytes (73), precluding the presentation of p40^{phox} dysfunction as CGD. This argument is

not supported by our initial characterization of p40^{phox} expression in the p40$^{phox-/-}$ mice, which did not provide evidence for high expression of p40^{phox} outside the haemopoetic system, nor by the fact that p40$^{phox-/-}$ mice appear healthy when raised under pathogen-free conditions. It seems plausible that either a loss of p40^{phox} presents a mild phenotype in humans or, indeed, that several uncharacterized cases of CGD-like immunodeficiencies may arise from as yet undescribed mutations in the p40^{phox} gene.

MATERIALS AND METHODS

Murine GM-CSF (mGM-CSF), FMLP, luminol, DPI, and HRP were from Sigma-Aldrich. Murine TNF-α (mTNF-α) was from R&D Systems. All buffer components were from Sigma-Aldrich and were endotoxin free or low endotoxin, as available. The following antibodies were used: anti–phospho-Ser473 PKB (Ab4802; Abcam), anti-PKB (9272; Cell Signaling), anti–phospho-T180/Y182 p38 (9211S; Cell Signaling), anti-p38 (9212; Cell Signaling), anti–phospho-T202/Y204 p42/44 (9106S; Cell Signaling), and anti-p42/22 (606-259-1550; TransLabs).

Generation of p40$^{phox-/-}$ mice. Several clones encoding the p40^{phox} genomic sequence were isolated from the RPCI mouse PAC library 21 (Pieter de Jong, UK HGMP Resource Centre) by Southern screens using an NT-cDNA probe. An 11.9-kb SpeI–SpeI fragment encompassing exons 1–4 was isolated from clone RP21-641C7 and inserted into the low copy number plasmid pSC-3Z to form the basis of a p40^{phox} gene-targeting vector (Fig. S1 A).

A smaller fragment containing exon 3 was subcloned into pBS, and site-directed mutagenesis was conducted to alter codon 73 to a translational stop and to introduce silent mutations creating additional XhoI and ApaI sites (Fig. S1 B), which were used to track the presence of the mutated sequence. This modified segment was sequenced and reintroduced into the targeting vector. This strategy was adopted because the translational stop or p40$^{phox-/-}$ mouse described here was one of several knock-in mutations planned for exon 3.

A loxP-flanked cassette containing a tACE-Cre expression module and a Neo^{R} expression module (pACN; A. Plagge, Babraham Institute, Cambridge, UK) (74) was inserted into the SnaBI site in the intron between exons 3 and 4 (Fig. S1 A). The tACE promoter is expected to operate in the testis and drive Cre/Lox-mediated deletion of this cassette on the breeding of targeted chimeras. Deletion is predicted to leave 59 bp of foreign DNA remaining in the intron.

The final targeting vector was digested with DraI and SalI (in the 3′ polylinker) to remove excess pSC-3Z vector sequence and used to transfect E14 129$^{s/v}$ embryonic stem cells by the Gene-Targeting Facility at the Babraham Institute. 500 clones were initially screened for homologous recombination using a 3′ Southern screen (probe 3′ to targeted sequence, EcoRI digest, 4.6–8.3 kb transition), and positive clones were rescreened by a 5′ Southern screen (probe 5′ to targeted sequence, SpeI digest, 11.9–10.0 kb transition) and for single insertion of the Neo^{R} cassette (Neo probe, EcoRI/8.3 kb, and SpeI/5.7 kb; Fig. S1, A and C). Three clones were taken forward for blastocyst injection, and male chimeras from these mice were bred with female C57BL/6 animals to generate p40$^{phox+/-}$ heterozygotes on a mixed 129$^{s/v}$/C57BL/6 background. Deletion of the Neo^{R} cassette was confirmed by appropriate Southern and PCR analyses, and separate p40$^{phox-/-}$ colonies were created from each of the original targeted embryonic stem cell lines and housed under specific pathogen-free conditions in the SABU facility at the Babraham Institute. Genotyping of the mice was routinely performed by PCR amplification of an approximately 850-bp region flanking exon 3 (to include the inserted translational stop and additional XhoI and ApaI sites) and subsequent diagnosis by susceptibility of the product to cleavage by XhoI or ApaI (to yield ∼525- and 325-bp fragments; Fig. S1 D). All mice used were 2–8-mo old and showed no age-dependent variation. This work was covered by UK Home Office Project License PPL 80/1875.

Preparation of BMNs. BMNs were prepared as described previously with minor modifications (75). Bone marrow, from at least three mice per preparation, was dispersed in HBSS (without Ca^{2+} and Mg^{2+}), 0.25% fatty acid–free BSA, 15 mM Hepes, pH7.4, at room temperature and purified over discontinuous Percoll (GE Healthcare) gradients. After washes, mature neutrophils were resuspended in Dulbecco's PBS with Ca^{2+} and Mg^{2+}, 1 g/liter glucose, 4 mM sodium bicarbonate (DPBS^{+}). Purity was typically 70–80% as assessed by cytospin and REASTAIN Quick-Diff (Reagena) staining (non-neutrophils were ∼50% immature white cells, 25% monocytes, and 25% lymphocytes). All assays were performed in DPBS^{+}. BMNs were primed at 37°C with 500 U/ml mTNF-α, 100 ng/ml mGM-CSF, and 10% mouse serum for 60 min. In some experiments, as indicated, BMNs were primed individually with 500 U/ml mTNF-α for 30 min, 100 ng/ml mGM-CSF for 60 min, or 500 U/ml mTNF-α and 100 ng/ml mGM-CSF for 60 min.

Neutrophil and multiple tissue Western blots. 5×10^6 BMNs were sonicated into 1× SDS loading buffer, and 5×10^5 cell equivalents were subjected to SDS-PAGE, transferred, and blotted for p40^{phox} (05-539 monoclonal; Upstate Biotechnology; sc-18252 and sc-18253 polyclonals; Santa Cruz Biotechnology, Inc.), p47^{phox} (07-500 polyclonal; Upstate Biotechnology), and p67^{phox} (07-502 polyclonal; Upstate Biotechnology). Signal was detected (Image Reader LAS-1000; Fugifilm) and quantified using Aida Image Analyser 2.2. For tissue Westerns, tissues were collected and immediately machinated into ice-cold 20 mM Hepes, pH7.1, at 4°C, 0.1% SDS, 0.4% cholate, 0.1% NP-40, 0.1M NaCl, 0.2 mM PMSF, and 10 μg/ml each of pepstatin A, leupeptin, antipain, and aprotinin and clarified by centrifugation (14,000 *g* for 30 min at 4°C). Protein concentrations were determined (BCA; Pierce Chemical Co.), and 30 μg of each protein was subjected to SDS-PAGE, transferred, and immunoblotted for p40^{phox}.

PKB, p38 MAPK, and p42/44 Erk activation assays. 5×10^6 unprimed BMNs from p40$^{phox-/-}$ and p40$^{phox+/+}$ mice were prewarmed for 3 min at 37°C at 5×10^7/ml in DPBS^{+} in duplicate. After 1 min of stimulation with prewarmed FMLP (10 μM final) or salts, reactions were stopped by the addition of excess ice-cold PBS, followed by immediate centrifugation (12,000 *g* for 10 s). Cell pellets were lysed in 20 mM Tris, pH 7.5 at 4°C, 150 mM NaCl, 1 mM EDTA, 1 mM EGTA, 1% Triton X-100, 2.5 mM sodium pyrophosphate, 1 mM β-glycerophosphate, 1 mM sodium orthovanadate, 0.2 mM PMSF, and 10 μg/ml each of pepstatin A, leupeptin, antipain, and aprotinin and incubated on ice for 10 min. Cytoskeletal debris was removed by centrifugation (12,000 *g* for 20 min at 4°C). Lysates were split between two SDS-PAGE gels and blotted for phospho- and total protein, respectively. Blots were imaged and quantified as described above.

Preparation of mouse serum. Mouse blood was collected and left to clot at room temperature for 45 min in a glass container before transferal to a 15-ml tube followed by centrifugation (1,500 *g* for 10 min at room temperature). Serum was removed to a fresh tube, recentrifuged, recovered, placed on ice, aliquoted, and stored at −80°C.

Chemiluminescent detection of ROS. ROS production was measured by luminol-dependent chemiluminescence in polystyrene 96-well plates (no. 23300; Berthold Technologies Ltd.) as described previously (75) in DPBS^{+}, except final concentrations of luminol and HRP were 150 μM and 18.75 U/ml, respectively. Prewarmed stimuli were added manually and measurement started immediately. Assays using soluble stimuli (PMA, FMLP, and mTNF-α) were conducted in the presence of exogenous added HRP; the signal was >95% HRP dependent, indicating predominantly extracellular ROS production (unpublished data). Assays using particulate stimuli (zymosan, IgG latex beads, and live *S. aureus*) were conducted without HRP and thus represent intracellular ROS production. The addition of HRP revealed little extracellular ROS production (unpublished data). Final particle/BMN ratios were as follows: zymosan, 5:1; *S. aureus*, 20:1; and IgG latex beads, 50:1. In some *S. aureus* experiments, BMNs were preincubated

with varying concentrations of DPI or vehicle (DMSO) alone before stimulation. Data output is in relative light units per second (rlu/s).

Adhesion-dependent responses. Surfaces (96-well plates or 12-well tissue culture plates) were coated overnight at 4°C with sheep fibrinogen (F9754; Sigma-Aldrich) at 150 μg/ml in PBS (100% FCS was used as a nonspecific control). Before use, surfaces were washed three times with PBS. For adhesion-dependent ROS assays, neutrophils at 5×10^6/ml were incubated at 37°C for 1 h before the addition of prewarmed 2× HRP/luminol followed by mTNF-α (final concentration of 20 ng/ml), anti-CD18 (anti–β2 integrin, M18/2; Chemicon), or IgG2a isotype control antibodies (final concentration of 18 μg/ml). Cells were immediately aliquoted into the plate (100 μl/well) and counted. For spreading experiments, preincubated neutrophils were incubated at 37°C in coated 12-well tissue culture plates (6.25×10^5/well) in the presence of 20 ng/ml mTNF-α. After 40 min, wells were aspirated and cells were fixed in 3.8% formaldehyde. Nonadhered cells were washed away and remaining cells were visualized by light microscopy. In both ROS and spreading assays, FCS-coated wells produced minimal responses (unpublished data). For analysis of β2 integrin expression, neutrophils were stimulated with mTNF-α for 30 min at 37°C, placed on ice, and processed for FACS analysis using the anti-CD18 antibody, its isotype control, and an FITC anti–rat secondary.

Preparation of particulate stimuli. IgG-opsonized zymosan particles (IgG-Zym) were prepared as per the manufacturer's instructions (unlabeled zymosan A, Z-2849, and rabbit anti-zymosan A, Z-2850; Invitrogen). Zymosan and *S. aureus* were serum opsonized or mock opsonized by incubation in $DPBS^+$ with or without 50% mouse serum at 37°C with end-over-end mixing for 1 h (zymosan) or 15 min (*S. aureus*) followed by washing. Carboxylate-modified latex beads (0.9-μm diameter; Sigma-Aldrich) were cross-linked to sulfhydryl-modified BSA and coated with an anti-BSA monoclonal antibody (Sigma-Aldrich) or not, as described previously (IgG latex beads) (76). Where appropriate, *S. aureus* was washed and resuspended in $DPBS^+$ (4×10^8/ml), heat killed at 60°C for 30 min, and opsonized in mouse serum as described above.

***S. aureus* phagocytosis assay.** 10^6 primed BMNs were allowed to adhere to glass coverslips for 20 min at 37°C. They were then aspirated, 10^7 FITC-labeled, serum-opsonized *S. aureus* was added, and they were returned to 37°C (FITC labeling of bacteria as described previously [77] and opsonization as detailed above). After 40 min, coverslips were washed, fixed in 4% paraformaldehyde, and mounted. Postfixation probing with a rabbit anti–*S. aureus* antibody (S-2860; Invitrogen) and goat anti–rabbit Alexa Fluor 568 secondary antibody (Invitrogen) revealed that >95% of bacteria present were internalized. Phagocytosed bacteria were visualized by fluorescence microscopy and enumerated.

Oxygen consumption. Oxygen consumption was measured in a Clark-type oxygen electrode (Rank Brothers Ltd.) at 37°C with rapid stirring. Primed BMNs were added to the rapidly stirred chamber at 5×10^6/ml and equilibrated for 5 min before the addition of prewarmed stimuli. Final concentrations were 1 μM PMA; IgG-Zym, 20:1; and heat-killed *S. aureus*, 20:1 (particles/BMNs).

NBT microscopy. Primed BMNs were adhered to a coverslip in 0.5 mg/ml NBT at 37°C. IgG-Zym particles were added, and dark purple formazan deposition was followed during phagocytosis by bright field microscopy.

In vitro bacterial killing assays. Bacteria (*S. aureus* Wood 46 and *E. coli* E2348169) were subcultured at 37°C to logarithmic growth from an overnight culture. 4×10^7 bacteria were washed in $DPBS^+$ and opsonized as described above. Opsonized bacteria (1.5×10^6 *S. aureus* and 6×10^6 *E. coli*) were added to 6.2×10^6 primed BMNs (2.5×10^7/ml) at 37°C with rapid orbital mixing. After the indicated times, 50-μl aliquots were removed to 950-μl ice-cold Luria broth (LB) containing 0.05% saponin. Samples were sonicated (output 1.5 for 10 s; Sonicator 3000; Misonix) to liberate intracellular bacteria and returned to ice. Suspensions were serially diluted and plated on LB-agar to enumerate surviving bacteria. A parallel bacterial incubation was also run in the absence of neutrophils. In some experiments, neutrophils were incubated for 5 min with DPI at varying concentrations or vehicle (DMSO) alone before the addition of bacteria (oxidant-dependent killing control).

For *S. aureus* killing assays in whole blood, 2.5×10^6 bacteria in 1 ml $DPBS^+$ were added to 1 ml of fresh whole blood (mixed from at least three animals) and incubated for 20 min at 37°C with end-over-end mixing. 0.8 ml of blood/bacteria mix was added to tubes containing lysostaphin (a final concentration of 2.5 U/ml to kill extracellular bacteria) in duplicate and returned to mixing. Samples were taken after 1 h, added to ice-cold PBS, and pelleted by centrifugation, and the pellets were resuspended in 0.5 ml nutrient broth, 0.05% saponin. Samples were then processed and quantified as described above.

In vivo *S. aureus* survival assays. S. aureus (LS-1) was subcultured at 37°C to logarithmic growth from an overnight culture. Bacteria were washed and resuspended in injection-grade PBS at 2.5×10^8/ml. Three animals of each genotype per time point were injected intraperitoneally with 0.2 ml of bacterial suspension (5×10^7 bacteria). After 4 or 24 h, mice were killed and the peritoneal cavity was thoroughly flushed with 10 ml ice-cold PBS, 5 mM EDTA, and 5 U/ml heparin. Aliquots were diluted, sonicated, and plated, and bacteria were enumerated as for the in vitro killing assays.

Online supplemental material. Fig. S1 illustrates the targeting strategy used to generate $p40^{phox-/-}$ mice and the subsequent screening strategies used. Fig. S2 denotes normal organ weights of $p40^{phox-/-}$ animals. Fig. S3 describes the *S. aureus* killing deficiency of whole blood from $p40^{phox-/-}$ animals.

We thank Ted Saunders, Martin George, and Debbie Drage of the Gene-Targeting Facility at Babraham for their excellent support; members of the Small Animal Breeding Unit at Babraham for animal husbandry; and Simon Andrews of the Bioinformatics group at Babraham for his help in the design of the gene-targeting strategy. We also thank Stephanie Brown and Michael Murphy for help and advice with oxygen electrode measurements (MRC-Dunn Human Nutrition Unit, Cambridge) and the laboratory of Anthony Green (Dept. of Haematology, Cambridge University) for use of their animal blood cell counter.

This work was supported by grants from the Biotechnology and Biological Sciences Research Council and Arthritis Research Council (no. S0679). C.D. Ellson is a Beit Memorial Fellow.

The authors have no conflicting financial interests.

Submitted: 14 October 2005
Accepted: 20 June 2006

REFERENCES

1. Cross, A.R., and A.W. Segal. 2004. The NADPH oxidase of professional phagocytes–prototype of the NOX electron transport chain systems. *Biochim. Biophys. Acta.* 1657:1–22.
2. Quinn, M.T., and K.A. Gauss. 2004. Structure and regulation of the neutrophil respiratory burst oxidase: comparison with nonphagocyte oxidases. *J. Leukoc. Biol.* 76:760–781.
3. Reeves, E.P., H. Lu, H.L. Jacobs, C.G. Messina, S. Bolsover, G. Gabella, E.O. Potma, A. Warley, J. Roes, and A.W. Segal. 2002. Killing activity of neutrophils is mediated through activation of proteases by K+ flux. *Nature.* 416:291–297.
4. Hampton, M.B., A.J. Kettle, and C.C. Winterbourn. 1998. Inside the neutrophil phagosome: oxidants, myeloperoxidase, and bacterial killing. *Blood.* 92:3007–3017.
5. Lambeth, J.D. 2004. NOX enzymes and the biology of reactive oxygen. *Nat. Rev. Immunol.* 4:181–189.
6. Lehrer, R.I. 2004. Primate defensins. *Nat. Rev. Microbiol.* 2:727–738.
7. Geiszt, M., and T.L. Leto. 2004. The Nox family of NAD(P)H oxidases: host defense and beyond. *J. Biol. Chem.* 279:51715–51718.

8. Tonks, N.K. 2005. Redox redux: revisiting PTPs and the control of cell signaling. *Cell*. 121:667–670.
9. Meischl, C., and D. Roos. 1998. The molecular basis of chronic granulomatous disease. *Springer Semin. Immunopathol.* 19:417–434.
10. Heyworth, P.G., A.R. Cross, and J.T. Curnutte. 2003. Chronic granulomatous disease. *Curr. Opin. Immunol.* 15:578–584.
11. Gu, Y., B. Jia, F.C. Yang, M. D'Souza, C.E. Harris, C.W. Derrow, Y. Zheng, and D.A. Williams. 2001. Biochemical and biological characterization of a human Rac2 GTPase mutant associated with phagocytic immunodeficiency. *J. Biol. Chem.* 276:15929–15938.
12. Groemping, Y., and K. Rittinger. 2005. Activation and assembly of the NADPH oxidase: a structural perspective. *Biochem. J.* 386:401–416.
13. Greenberg, S., and S. Grinstein. 2002. Phagocytosis and innate immunity. *Curr. Opin. Immunol.* 14:136–145.
14. Mayer-Scholl, A., P. Averhoff, and A. Zychlinsky. 2004. How do neutrophils and pathogens interact? *Curr. Opin. Microbiol.* 7:62–66.
15. Sheppard, F.R., M.R. Kelher, E.E. Moore, N.J. McLaughlin, A. Banerjee, and C.C. Silliman. 2005. Structural organization of the neutrophil NADPH oxidase: phosphorylation and translocation during priming and activation. *J. Leukoc. Biol.* 78:1025–1042.
16. Dewald, B., M. Thelen, and M. Baggiolini. 1988. Two transduction sequences are necessary for neutrophil activation by receptor agonists. *J. Biol. Chem.* 263:16179–16184.
17. McPhail, L.C., C.C. Clayton, and R. Snyderman. 1984. The NADPH oxidase of human polymorphonuclear leukocytes. Evidence for regulation by multiple signals. *J. Biol. Chem.* 259:5768–5775.
18. Kim, C., C.C. Marchal, J. Penninger, and M.C. Dinauer. 2003. The hemopoietic Rho/Rac guanine nucleotide exchange factor Vav1 regulates N-formyl-methionyl-leucyl-phenylalanine-activated neutrophil functions. *J. Immunol.* 171:4425–4430.
19. Price, M.O., S.J. Atkinson, U.G. Knaus, and M.C. Dinauer. 2002. Rac activation induces NADPH oxidase activity in transgenic COSphox cells, and the level of superoxide production is exchange factor-dependent. *J. Biol. Chem.* 277:19220–19228.
20. Welch, H.C., W.J. Coadwell, C.D. Ellson, G.J. Ferguson, S.R. Andrews, H. Erdjument-Bromage, P. Tempst, P.T. Hawkins, and L.R. Stephens. 2002. P-Rex1, a PtdIns(3,4,5)P3- and Gbetagamma-regulated guanine-nucleotide exchange factor for Rac. *Cell*. 108:809–821.
21. Dinauer, M.C. 2003. Regulation of neutrophil function by Rac GTPases. *Curr. Opin. Hematol.* 10:8–15.
22. Brown, G.E., M.Q. Stewart, H. Liu, V.L. Ha, and M.B. Yaffe. 2003. A novel assay system implicates PtdIns(3,4)P(2), PtdIns(3)P, and PKC delta in intracellular production of reactive oxygen species by the NADPH oxidase. *Mol. Cell.* 11:35–47.
23. Dang, P.M., A. Fontayne, J. Hakim, J. El Benna, and A. Perianin. 2001. Protein kinase C zeta phosphorylates a subset of selective sites of the NADPH oxidase component p47phox and participates in formyl peptide-mediated neutrophil respiratory burst. *J. Immunol.* 166:1206–1213.
24. Fontayne, A., P.M. Dang, M.A. Gougerot-Pocidalo, and J. El-Benna. 2002. Phosphorylation of p47phox sites by PKC alpha, beta II, delta, and zeta: effect on binding to p22phox and on NADPH oxidase activation. *Biochemistry*. 41:7743–7750.
25. Brown, G.E., M.Q. Stewart, S.A. Bissonnette, A.E. Elia, E. Wilker, and M.B. Yaffe. 2004. Distinct ligand-dependent roles for p38 MAPK in priming and activation of the neutrophil NADPH oxidase. *J. Biol. Chem.* 279:27059–27068.
26. Dang, P.M., F. Morel, M.A. Gougerot-Pocidalo, and J.E. Benna. 2003. Phosphorylation of the NADPH oxidase component p67(PHOX) by ERK2 and P38MAPK: selectivity of phosphorylated sites and existence of an intramolecular regulatory domain in the tetratricopeptide-rich region. *Biochemistry*. 42:4520–4526.
27. Guichard, C., E. Pedruzzi, C. Dewas, M. Fay, C. Pouzet, M. Bens, A. Vandewalle, E. Ogier-Denis, M.A. Gougerot-Pocidalo, and C. Elbim. 2005. Interleukin-8-induced priming of the neutrophil oxidative burst requires sequential recruitment of NADPH oxidase components into lipid rafts. *J. Biol. Chem.* 280:37021–37032.
28. Coffer, P.J., N. Geijsen, L. M'rabet, R.C. Schweizer, T. Maikoe, J.A. Raaijmakers, J.W. Lammers, and L. Koenderman. 1998. Comparison of the roles of mitogen-activated protein kinase kinase and phosphatidylinositol 3-kinase signal transduction in neutrophil effector function. *Biochem. J.* 329:121–130.
29. Yamamori, T., O. Inanami, H. Nagahata, and M. Kuwabara. 2004. Phosphoinositide 3-kinase regulates the phosphorylation of NADPH oxidase component p47(phox) by controlling cPKC/PKCdelta but not Akt. *Biochem. Biophys. Res. Commun.* 316:720–730.
30. Ago, T., F. Kuribayashi, H. Hiroaki, R. Takeya, T. Ito, D. Kohda, and H. Sumimoto. 2003. Phosphorylation of p47phox directs phox homology domain from SH3 domain toward phosphoinositides, leading to phagocyte NADPH oxidase activation. *Proc. Natl. Acad. Sci. USA*. 100:4474–4479.
31. Karathanassis, D., R.V. Stahelin, J. Bravo, O. Perisic, C.M. Pacold, W. Cho, and R.L. Williams. 2002. Binding of the PX domain of p47(phox) to phosphatidylinositol 3,4-bisphosphate and phosphatidic acid is masked by an intramolecular interaction. *EMBO J.* 21:5057–5068.
32. Wilson, M.I., D.J. Gill, O. Perisic, M.T. Quinn, and R.L. Williams. 2003. PB1 domain-mediated heterodimerization in NADPH oxidase and signaling complexes of atypical protein kinase C with Par6 and p62. *Mol. Cell.* 12:39–50.
33. Ito, T., Y. Matsui, T. Ago, K. Ota, and H. Sumimoto. 2001. Novel modular domain PB1 recognizes PC motif to mediate functional protein-protein interactions. *EMBO J.* 20:3938–3946.
34. Wientjes, F.B., J.J. Hsuan, N.F. Totty, and A.W. Segal. 1993. p40phox, a third cytosolic component of the activation complex of the NADPH oxidase to contain src homology 3 domains. *Biochem. J.* 296:557–561.
35. Someya, A., I. Nagaoka, and T. Yamashita. 1993. Purification of the 260 kDa cytosolic complex involved in the superoxide production of guinea pig neutrophils. *FEBS Lett.* 330:215–218.
36. Lapouge, K., S.J. Smith, Y. Groemping, and K. Rittinger. 2002. Architecture of the p40-p47-p67phox complex in the resting state of the NADPH oxidase. A central role for p67phox. *J. Biol. Chem.* 277:10121–10128.
37. Ellson, C.D., S. Gobert-Gosse, K.E. Anderson, K. Davidson, H. Erdjument-Bromage, P. Tempst, J.W. Thuring, M.A. Cooper, Z.Y. Lim, A.B. Holmes, et al. 2001. PtdIns(3)P regulates the neutrophil oxidase complex by binding to the PX domain of p40(phox). *Nat. Cell Biol.* 3:679–682.
38. Cross, A.R. 2000. p40(phox) participates in the activation of NADPH oxidase by increasing the affinity of p47(phox) for flavocytochrome b(558). *Biochem. J.* 349:113–117.
39. Tsunawaki, S., S. Kagara, K. Yoshikawa, L.S. Yoshida, T. Kuratsuji, and H. Namiki. 1996. Involvement of p40phox in activation of phagocyte NADPH oxidase through association of its carboxyl-terminal, but not its amino-terminal, with p67phox. *J. Exp. Med.* 184:893–902.
40. Lopes, L.R., M.C. Dagher, A. Gutierrez, B. Young, A.P. Bouin, A. Fuchs, and B.M. Babior. 2004. Phosphorylated p40PHOX as a negative regulator of NADPH oxidase. *Biochemistry*. 43:3723–3730.
41. He, R., M. Nanamori, H. Sang, H. Yin, M.C. Dinauer, and R.D. Ye. 2004. Reconstitution of chemotactic peptide-induced nicotinamide adenine dinucleotide phosphate (reduced) oxidase activation in transgenic COS-phox cells. *J. Immunol.* 173:7462–7470.
42. Sathyamoorthy, M., I. de Mendez, A.G. Adams, and T.L. Leto. 1997. p40(phox) down-regulates NADPH oxidase activity through interactions with its SH3 domain. *J. Biol. Chem.* 272:9141–9146.
43. Kuribayashi, F., H. Nunoi, K. Wakamatsu, S. Tsunawaki, K. Sato, T. Ito, and H. Sumimoto. 2002. The adaptor protein p40(phox) as a positive regulator of the superoxide-producing phagocyte oxidase. *EMBO J.* 21:6312–6320.
44. Someya, A., H. Nunoi, T. Hasebe, and I. Nagaoka. 1999. Phosphorylation of p40-phox during activation of neutrophil NADPH oxidase. *J. Leukoc. Biol.* 66:851–857.
45. Bouin, A.P., N. Grandvaux, P.V. Vignais, and A. Fuchs. 1998. p40(phox) is phosphorylated on threonine 154 and serine 315 during activation of the phagocyte NADPH oxidase. Implication of a protein kinase c-type kinase in the phosphorylation process. *J. Biol. Chem.* 273:30097–30103.
46. Kanai, F., H. Liu, S.J. Field, H. Akbary, T. Matsuo, G.E. Brown, L.C. Cantley, and M.B. Yaffe. 2001. The PX domains of p47phox and p40phox bind to lipid products of PI(3). *Nat. Cell Biol.* 3:675–678.

47. Ago, T., R. Takeya, H. Hiroaki, F. Kuribayashi, T. Ito, D. Kohda, and H. Sumimoto. 2001. The PX domain as a novel phosphoinositide-binding module. *Biochem. Biophys. Res. Commun.* 287:733–738.
48. Fuchs, A., M.C. Dagher, and P.V. Vignais. 1995. Mapping the domains of interaction of p40phox with both p47phox and p67phox of the neutrophil oxidase complex using the two-hybrid system. *J. Biol. Chem.* 270:5695–5697.
49. Morozov, I., O. Lotan, G. Joseph, Y. Gorzalczany, and E. Pick. 1998. Mapping of functional domains in p47(phox) involved in the activation of NADPH oxidase by "peptide walking". *J. Biol. Chem.* 273:15435–15444.
50. Wientjes, F.B., E.P. Reeves, V. Soskic, H. Furthmayr, and A.W. Segal. 2001. The NADPH oxidase components p47(phox) and p40(phox) bind to moesin through their PX domain. *Biochem. Biophys. Res. Commun.* 289:382–388.
51. Grogan, A., E. Reeves, N. Keep, F. Wientjes, N.F. Totty, A.L. Burlingame, J.J. Hsuan, and A.W. Segal. 1997. Cytosolic phox proteins interact with and regulate the assembly of coronin in neutrophils. *J. Cell Sci.* 110:3071–3081.
52. Nishiyama, A., T. Ohno, S. Iwata, M. Matsui, K. Hirota, H. Masutani, H. Nakamura, and J. Yodoi. 1999. Demonstration of the interaction of thioredoxin with p40phox, a phagocyte oxidase component, using a yeast two-hybrid system. *Immunol. Lett.* 68:155–159.
53. Grandvaux, N., S. Grizot, P.V. Vignais, and M.C. Dagher. 1999. The Ku70 autoantigen interacts with p40phox in B lymphocytes. *J. Cell Sci.* 112:503–513.
54. Dahlgren, C., and A. Karlsson. 1999. Respiratory burst in human neutrophils. *J. Immunol. Methods.* 232:3–14.
55. Reiss, M., and D. Roos. 1978. Differences in oxygen metabolism of phagocytosing monocytes and neutrophils. *J. Clin. Invest.* 61:480–488.
56. Nathan, C.F. 1987. Neutrophil activation on biological surfaces: massive secretion of hydrogen peroxide in response to products of macrophages and lymphocytes. *J. Clin. Invest.* 80:1550–1560.
57. Lowell, C.A., L. Fumagalli, and G. Berton. 1996. Deficiency of Src family kinases p59/61*hck* and p58*c-fgr* results in defective adhesion-dependent neutrophil functions. *J. Cell Biol.* 133:895–910.
58. Jakus, Z., G. Berton, E. Ligeti, C.A. Lowell, and A. Mocsai. 2004. Responses of neutrophils to anti-integrin antibodies depends on costimulation through low affinity Fc-gammaRs: full activation requires both integrin and nonintegrin signals. *J. Immunol.* 173:2068–2077.
59. Nathan, C., S. Srimal, C. Farber, E. Sanchez, L. Kabbash, A. Asch, J. Gailit, and S.D. Wright. 1989. Cytokine-induced respiratory burst of human neutrophils: dependence on extracellular matrix proteins and CD11/CD18 integrins. *J. Cell Biol.* 109:1341–1349.
60. Mócsai, A., M. Zhou, F. Meng, V.L. Tybulewicz, and C.A. Lowell. 2002. Syk is required for integrin signaling in neutrophils. *Immunity.* 16:547–548.
61. Rada, B.K., M. Geiszt, K. Kaldi, C. Timar, and E. Ligeti. 2004. Dual role of phagocytic NADPH oxidase in bacterial killing. *Blood.* 104:2947–2953.
62. Richter, J., U. Gullberg, and M. Lantz. 1995. TNF-induced superoxide anion production in adherent human neutrophils involves both the p55 and p75 TNF receptor. *J. Immunol.* 154:4142–4149.
63. Fu, H., J. Bylund, A. Karlsson, S. Pellme, and C. Dahlgren. 2004. The mechanism for activation of the neutrophil NADPH-oxidase by the peptides formyl-Met-Leu-Phe and Trp-Lys-Tyr-Met-Val-Met differs from that for interleukin-8. *Immunology.* 112:201–210.
64. Zhou, M.J., and E.J. Brown. 1994. CR3 (Mac-1, $\alpha_M\beta_2$, CD11b/CD18) and FcγRIII cooperate in generation of a neutrophil respiratory burst: requirement for FcγRIII and tyrosine phosphorylation. *J. Cell Biol.* 125:1407–1416.
65. Gantner, B.N., R.M. Simmons, S.J. Canavera, S. Akira, and D.M. Underhill. 2003. Collaborative induction of inflammatory responses by dectin-1 and Toll-like receptor 2. *J. Exp. Med.* 197:1107–1117.
66. Jackson, S.H., J.I. Gallin, and S.M. Holland. 1995. The p47phox mouse knock-out model of chronic granulomatous disease. *J. Exp. Med.* 182:751–758.
67. Tsunawaki, S., H. Mizunari, M. Nagata, O. Tatsuzawa, and T. Kuratsuji. 1994. A novel cytosolic component, p40phox, of respiratory burst oxidase associates with p67phox and is absent in patients with chronic granulomatous disease who lack p67phox. *Biochem. Biophys. Res. Commun.* 199:1378–1387.
68. Dusi, S., M. Donini, and F. Rossi. 1996. Mechanisms of NADPH oxidase activation: translocation of p40phox, Rac1 and Rac2 from the cytosol to the membranes in human neutrophils lacking p47phox or p67phox. *Biochem. J.* 314:409–412.
69. de Boer, M., P.M. Hilarius-Stokman, J.P. Hossle, A.J. Verhoeven, N. Graf, R.T. Kenney, R. Seger, and D. Roos. 1994. Autosomal recessive chronic granulomatous disease with absence of the 67-kD cytosolic NADPH oxidase component: identification of mutation and detection of carriers. *Blood.* 83:531–536.
70. Ellson, C.D., K.E. Anderson, G. Morgan, E.R. Chilvers, P. Lipp, L.R. Stephens, and P.T. Hawkins. 2001. Phosphatidylinositol 3-phosphate is generated in phagosomal membranes. *Curr. Biol.* 11:1631–1635.
71. Vieira, O.V., R.J. Botelho, L. Rameh, S.M. Brachmann, T. Matsuo, H.W. Davidson, A. Schreiber, J.M. Backer, L.C. Cantley, and S. Grinstein. 2001. Distinct roles of class I and class III phosphatidylinositol 3-kinases in phagosome formation and maturation. *J. Cell Biol.* 155:19–25.
72. Suh, C.-I., N.D. Stull, X.J. Li, W. Tian, M.O. Price, S. Grinstein, M.B. Yaffe, S. Atkinson, and M.C. Dinauer. 2006. The phosphoinositide-binding protein $p40^{phox}$ activates the NADPH oxidase during FcγIIA receptor–induced phagocytosis. *J. Exp. Med.* 203:1915–1925.
73. Mizuki, K., K. Kadomatsu, K. Hata, T. Ito, Q.W. Fan, Y. Kage, Y. Fukumaki, Y. Sakaki, K. Takeshige, and H. Sumimoto. 1998. Functional modules and expression of mouse p40(phox) and p67(phox), SH3-domain-containing proteins involved in the phagocyte NADPH oxidase complex. *Eur. J. Biochem.* 251:573–582.
74. Bunting, M., K.E. Bernstein, J.M. Greer, M.R. Capecchi, and K.R. Thomas. 1999. Targeting genes for self-excision in the germ line. *Genes Dev.* 13:1524–1528.
75. Condliffe, A.M., K. Davidson, K.E. Anderson, C.D. Ellson, T. Crabbe, K. Okkenhaug, B. Vanhaesebroeck, M. Turner, L. Webb, M.P. Wymann, et al. 2005. Sequential activation of class IB and class IA PI3K is important for the primed respiratory burst of human but not murine neutrophils. *Blood.* 106:1432–1440.
76. Cox, D., C.C. Tseng, G. Bjekic, and S. Greenberg. 1999. A requirement for phosphatidylinositol 3-kinase in pseudopod extension. *J. Biol. Chem.* 274:1240–1247.
77. Rooijakkers, S.H., W.J. van Wamel, M. Ruyken, K.P. van Kessel, and J.A. van Strijp. 2005. Anti-opsonic properties of staphylokinase. *Microbes Infect.* 7:476–484.